Miniaturized microDMFC using silicon microsystems techniques: performances at low fuel flow rates

Ai Kamitani, Satoshi Morishita, Hiroshi Kotaki, S. Arscott

Miniaturized microDMFC using silicon microsystems techniques: performances at low fuel flow rates

Ai Kamitani[1], Satoshi Morishita[1], Hiroshi Kotaki[1] and Steve Arscott[2,3]

[1] Advanced Technology Research Laboratories, Corporate Research and Development Group, SHARP Corporation, 2613-1, Ichinomoto-cho, Tenri, Nara, 632-8567, Japan
[2] Institut d'Electronique, de Microélectronique et de Nanotechnologie (IEMN), CNRS UMR8520, University of Lille, Avenue Poincaré, Cite Scientifique, 59652 Villeneuve d'Ascq, France

E-mail: steve.arscott@iemn.univ-lille1.fr

Abstract

This paper reports the design, fabrication and characterization of high performance miniaturized micro direct methanol fuel cells (microDMFC) functioning at room temperature under a forced low input fuel flow rate (<10 μL min^{-1}) fabricated using silicon microsystems techniques. A room temperature maximum power output of 12.5 mW cm^{-2} has been measured at a fuel flow rate of 5.52 μL min^{-1} for a fuel cell surface area as small as 0.3 cm^2 (corresponding to a fuel use efficiency of 14.1% at 300 K). At a lower flow rate of 1.38 μL min^{-1}, the fuel use efficiency rises to 20.1% although the power density falls to 4.3 mW cm^{-2}. The study revealed that improved room temperature cell performances in terms of power density can be achieved at low flow rates (<10 μL min^{-1}) by (i) reducing the fuel cell area and (ii) reducing the microchannel cross-section. The study also revealed that higher fuel use efficiencies are obtained at lower fuel flow rates. Fuel (methanol) for the anode and an oxidant (air) for the cathode are supplied via a compact serpentine network of micron-size microfluidic and gas microchannels; by using silicon microsystems techniques we also render the fuel cell compatible with other silicon technologies such as microelectronics and micro- and nanoelectromechanical systems (MEMS/NEMS).

1. Introduction

Micro fuel cells [1] have potentially numerous applications ranging from powering all manners of small lightweight consumer portable electronic equipment [2] to being integrated on-chip energy sources for the current trends in autonomous micro- and nanoelectromechanical systems (MEMS/NEMS), and the compatibility of these systems with silicon microelectronics which could be useful for a whole host of sensors and actuators. Micro direct methanol fuel cells (microDMFC) [3, 4] are currently under investigation due to their potentially high energy density (4333 W h L^{-1}) compared to current galvanic batteries (lithium ion battery ~200 W h kg^{-1}) and liquid fuel storage advantages compared to, for example, the hydrogen fuel cell. In order to achieve high performance miniaturized microDMFCs, several problems must be solved; these include methanol crossover [5, 6], water flooding in the cathode channels [7], carbon dioxide bubble formation at the anode [8, 9], mass transport [10, 11] and fuel concentration [12] issues. In order to address the above issues, microfluidic technologies [13] can be applied for the miniaturization of fuel cells [14–16] via the use of microsystems technologies [17–30]. In 2000, Kelley *et al* [17] was the first group to apply silicon microsystems techniques to microDMFC, producing a system functioning at a high fuel flow rate of 2000 μL min^{-1}. This can be contrasted with Wozniak *et al* [20], who, using a network of silicon microchannels having a 100 μm depth for a 0.25 cm^2 surface fuel cell, reduced the flow rate to 0.16 μL min^{-1} resulting in

[1] Author to whom any correspondence should be addressed.

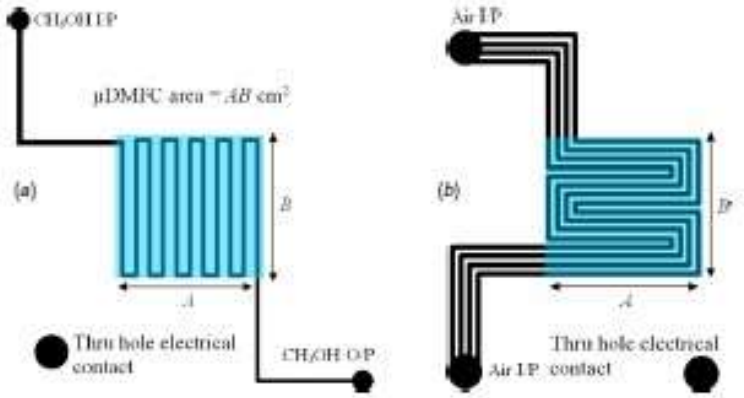

Figure 1. Fuel cell layout: (*a*) anode, (*b*) cathode. Serpentine microchannels etched in silicon wafers are shown in black; the effective fuel cell area is shown in blue; microfluidic and gas inputs/outputs are also shown.

a power output of ~0.3 mW cm^{-2}. Yen *et al* [18] achieved 47.2 mW cm^{-2} for a dry-etched silicon microchannel (750 μm width by 400 μm depth) operating at 60 °C, but this fell to 12 mW cm^{-2} at room temperature for a fuel flow rate of 283 μL min^{-1}. However, notable recent results are Wong *et al* [26] who demonstrated a power output of 34 mW cm^{-2} for a 1 cm^2 serpentine silicon microchannel-based system at a fuel flow rate of 800 μL min^{-1} and Zhang *et al* [28] who, using silicon microchannels in a novel microblock array, achieved a room temperature power density of 8.08 mW cm^{-2} at a fuel flow rate of 600 μL min^{-1}.

Here, we asses the room temperature performance of miniaturized microDMFCs (active fuel cell area $A < 0.4$ cm^2) at controlled forced fuel flow rates less than 10 μL min^{-1} fabricated using silicon microsystems technologies in the context of achieving a miniaturized high energy density fuel cell with a high fuel use efficiency for use as an on-chip integrated fuel cell compatible with silicon microsystems and microelectronics techniques.

2. Design

The fuel cell design implemented here is composed of (i) an anode microchannel, (ii) an anode diffusion layer, (iii) an anode electrode, (iv) a proton exchange membrane (PEM), (v) a cathode electrode, (vi) a cathode diffusion layer and (vii) a cathode microchannel. In terms of the anode, a single serpentine microchannel [26] was defined as shown in figure 1(*a*). The microchannel height h was equal to 50 and 100 μm, the channel width w equal to 50 μm and the channel length L equal to 6 cm (area $A = 0.18$ cm^2), 9 cm ($A = 0.3$ cm^2) and 12 cm ($A = 0.39$ cm^2), respectively. We define A here by taking into account the whole surface (the product AB indicated in figure 1(*a*)) including the microchannel spacing. Thru-holes are included in each pattern for the introduction of fuel and air and to provide electrical contacts to characterize the fuel cell. In terms of the cathode, four parallel serpentine channels were arranged in parallel as shown in figure 1(*b*). The channel height h, channel width w and channel length L were 150 μm, 200 μm and 4.67 cm, respectively.

2.1. Microfluidic considerations of the design

The anode silicon wafers contained microchannels having a hydrophilic silicon dioxide surface (contact angle θ_c of the 3 M methanol solution <10°) surrounded by a fluorocarbon hydrophobic surface deposited on the wafer surface ($\theta_c >$ 100°). When the wafer surface is in contact with the porous diffusion layer (θ_c of the 3 M methanol solution measured to be 134° and 107° after multi-use), the capillary filling between the two hydrophobic surfaces, i.e. fuel leaks, is not favourable as $\cos\theta_c < 0$; the pressure drop ΔP is given by the Young–Laplace equation ($\Delta P = 2\gamma\cos\theta_c/\delta$). If we take the surface energy of the fuel γ to be ~66 mJ m^{-2} and the space between the wafer and the diffusion layer δ to be 0.1 μm, $\Delta P >$ 0.2 MPa. For a microchannel having a length of 12 cm, a width of 50 μm and a height of 100 μm, the flow rate would need to exceed ~70 μL min^{-1} to achieve this pressure. It is important to predict the hydrodynamic pressure in the system which can lead to leaks (see above) and microfluidic connection problems. We know from the Hagen–Poiseuille equation for a rectangular microchannel that the volume flow rate Q is given by $Q = whD_h^2\Delta P/32\eta L$, $D_h = 2wh/[w+h]$, where η is the dynamic viscosity of the fuel, $\eta \sim 0.94$ mPa s. If we consider a microchannel having the smallest cross-section (50 μm × 50 μm) and the longest length (12 cm), then the pressure drop is <0.1 MPa (<1 bar) for a flow rate of 10 μL min^{-1}: this pressure is within the specifications of the microfluidic connections and is also lower than the leak pressure limit calculated above.

In terms of the cathode microchannels, we must consider water flooding. As the cathode diffusion layer is hydrophobic, water droplets are likely to be formed in the cathode microchannels. For a water droplet in the microchannel air flow, we have to consider (i) droplet motion and (ii) droplet evaporation. The former can be calculated by using a force balance of the Stokes force (low Reynolds number) and the droplet sticking force due to contact angle hysteresis [31]. If we assume a near spherical droplet (large contact angle), $6\eta v > \gamma\sin\theta_r(\cos\theta_r - \cos\theta_a)$ can be shown to have droplet motion, where η is the dynamic viscosity of air, v is the gas flow velocity in the microchannel, γ is the surface tension of the

Table 1. Fuel cell parameters used for the modelling.

Parameter	Value
T, cell temperature	300 K
D_{da}, diffusion coefficient of methanol in the anode diffusion layer	4.14×10^{-6} cm^2 s^{-1}
D_{dc}, diffusion coefficient of methanol in the cathode diffusion layer	2.4×10^{-1} cm^2 s^{-1}
d_{da}, thickness of the anode diffusion layer	235 μm
d_{dc}, thickness of the cathode diffusion layer	400 μm
C, methanol fuel concentration	3 M
η, viscosity of fuel	9.4×10^{-4} Pa s
D_m, diffusion coefficient of methanol in PEM	2.16×10^{-6} cm^2 s^{-1}
d_m, thickness of PEM	175 μm
α, electro-osmotic drag coefficient	2
$w_{\mu a}$, width of the anode microchannel	50 μm
$h_{\mu a}$, height of the anode microchannel	50 and 100 μm
$L_{\mu a}$, length of the anode microchannel	6, 9 and 12 cm (1 microchannel)
$w_{\mu c}$, width of the cathode microchannel	200
$h_{\mu c}$, height of the cathode microchannel	150
$L_{\mu c}$, length of the cathode microchannel	4.67 cm (4 microchannels)
A, fuel cell area	0.18, 0.3 and 0.39 cm^2
Q_a, anode input flow rate range	1.38–8.28 μL min^{-1}
Q_c, cathode input flow rate range	1–30 sccm

droplet, θ_c is the contact angle of water on the microchannel surface, and θ_r and θ_a are the receding and advancing contact angles; interestingly, the inequality is independent of the droplet size. Droplet evaporation in a gas flow has been described by $r^2(t) = r_0^2 - \beta t$ [32], where r_0 is the initial droplet radius and β is the evaporation coefficient (m^2 s^{-1}) at a given gas flow velocity v. Over the measured flow rates (5–30 sccm) and using four parallel cathode microchannels having dimensions 150 μm $\times$ 200 μm $\times$ 4.67 cm, the above reasoning predicts that droplet evaporation should be dominant. Droplet evaporation occurs in less than 1 s, using the coefficients given in [32], for a water droplet having a radius of a few tens of micrometres, whereas droplet motion only occurs if the contact angle hysteresis is very low, i.e. <1°; droplet motion could occur at higher air flow or larger contact angle, i.e. a superhydrophobic microchannel surface.

2.2. Cell performance

In order to predict the performances of the fuel cell we have implemented a multi-parameter 2D analytical model [33] which uses Fick's law and the Tafel equation. The model is based on rectangular microfluidic microchannels having a width w, a height h and a length L (subscripts: a = anode, c = cathode, μ = microchannel, d = diffusion layer and m = membrane) resting on porous diffusion layers having a thickness d which in turn rest on a PEM having a thickness d_m (see figure 2). Taking the example of the anode, we have

$$\frac{dc_{\mu a}}{dx} = -\frac{w_{\mu a}\Phi_{da}}{Q_{ia}} \tag{1}$$

$$\frac{\partial c_{da}}{\partial y} = -\frac{\Phi_{da}}{D_{da}} \tag{2}$$

where $c_{\mu a}$ is the methanol concentration along (x direction) the anode microchannel, $w_{\mu a}$ is the width of the anode microchannel, Φ_{da} (mol m^{-2} s^{-1}) is the methanol flux from the anode microchannel to the anode diffusion layer, Q_{ia} is the input flow rate in the anode microchannel, c_{da} is the molar methanol concentration through (y direction) the diffusion layer and D_{da} is the diffusion constant of methanol in the anode diffusion layer. In terms of the electrical performances, we have

$$\Phi_{da} = \frac{J_a}{6F} + \Phi_m \tag{3}$$

where

$$\Phi_m = -D_m\frac{\partial c_m}{\partial y} + \frac{\alpha J_a}{F} \tag{4}$$

where Φ_m (mol m^{-2} s^{-1}) is the methanol crossover flux, D_m is the diffusion coefficient of methanol in the PEM, c_m is the methanol concentration across the PEM, α is the electro-osmotic drag coefficient of methanol, J_a is the current density and F is the Faraday constant (96 485.33 C mol^{-1}). Analytical solutions [34–37] permit one to calculate the concentrations of methanol and oxygen present in the anode

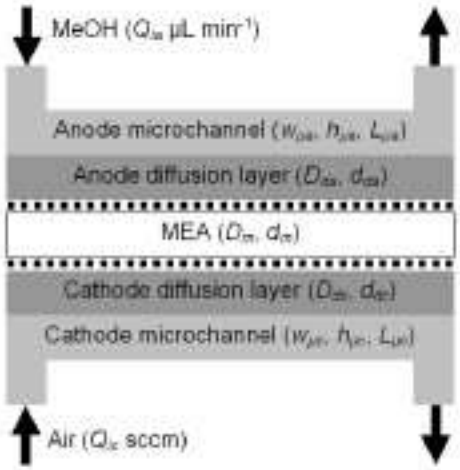

Figure 2. The fuel cell set-up used for the experiments also showing the important parameters used in the modelling.

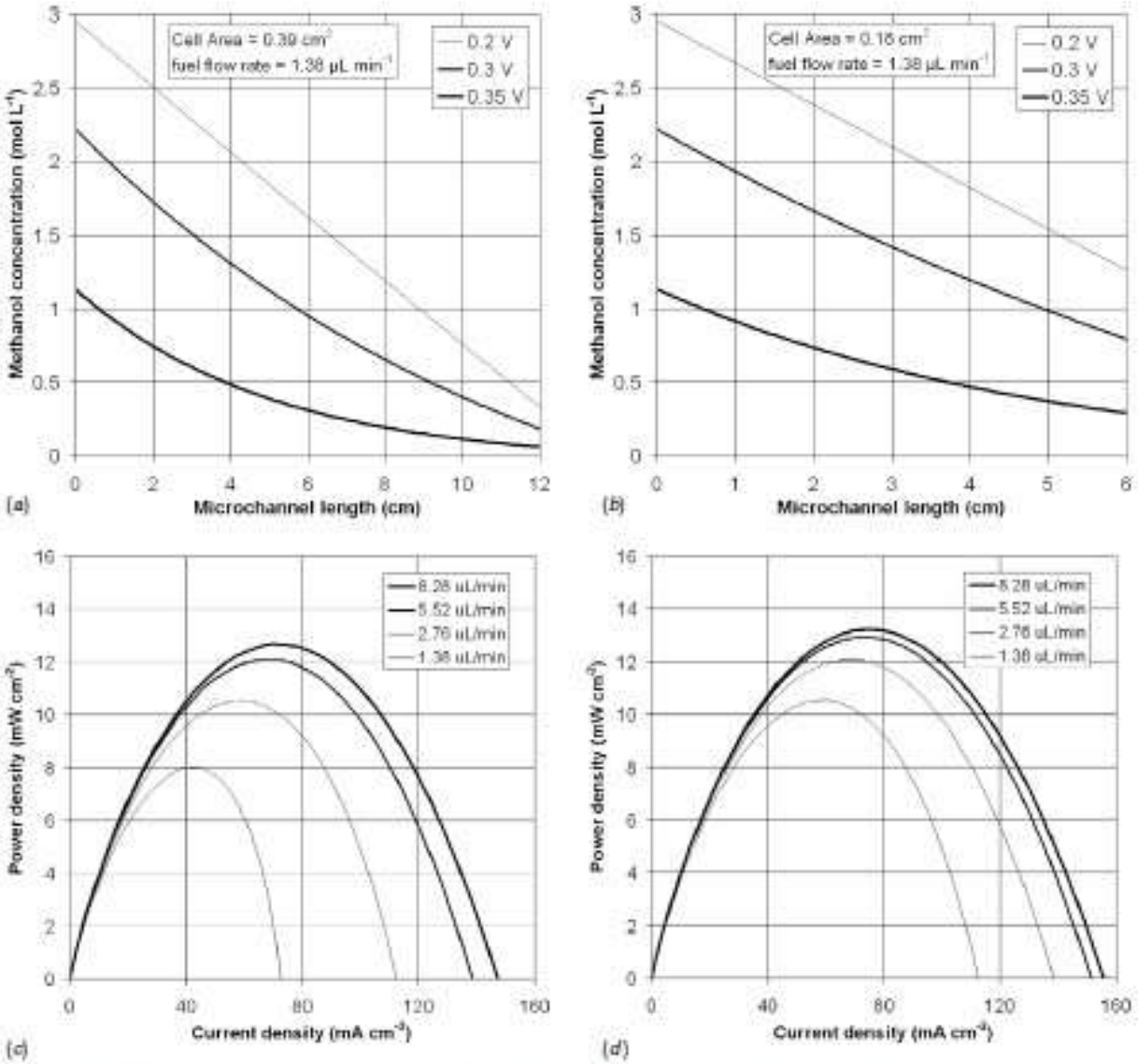

Figure 3. Calculated variation of the methanol concentration at the anode catalyst layer as a function of the microchannel length at different values of anode overpotential at a constant fuel flow rate of 1.38 μL min^{-1}: (*a*) $A = 0.39$ cm^2 and (*b*) $A = 0.18$ cm^2. Calculated fuel cell power output performances for (*c*) fuel flow variation at constant air flow (30 sccm), $A = 0.39$ cm^2, and (*d*) fuel flow variation at constant air flow (30 sccm), $A = 0.18$ cm^2.

and cathode microchannels and at the anode and cathode catalyst layers; from this the fuel cell's electrical performances can be predicted for a given set of fuel cell parameters. The parameters used in this study are listed in table 1. The model makes several assumptions including that the pressure drop is not taken into account; more details can be found in [33]. We initially verified the model by using the parameters given in [33]. The model does not take into consideration carbon dioxide generation, but despite this, the model demonstrates three important predictions: (a) at the fuel flow rates used, the output is a strong variation of the input fuel flow rate, (b) a low fuel flow rate (e.g. 1.38 μL min^{-1}) results in a low power output (e.g. ~2 mW cm^{-2}) at a cell area of 0.39 cm^2 even when carbon dioxide is not taken into account and (c) there is a power output saturation effect as a function of the input fuel rate. The analytical modelling allows one to verify the microchannel dimensions chosen based on the microfluidic considerations.

Figures 3(*a*) and (*b*) show the calculated variation of the methanol concentration at the anode catalyst layer as a function of the microchannel length at different values of anode overpotential at a constant fuel flow rate of 8.28 μL min^{-1} for two different fuel cells. The model predicts that the methanol concentration decreases with length and also decreases as the anode overpotential increases. Also for a larger area fuel cell, the fuel cell needs will not be met for a certain length of microchannel under certain operating conditions (flow rate and anode overpotential). Figures 3(*c*) and (*d*) show the modelled

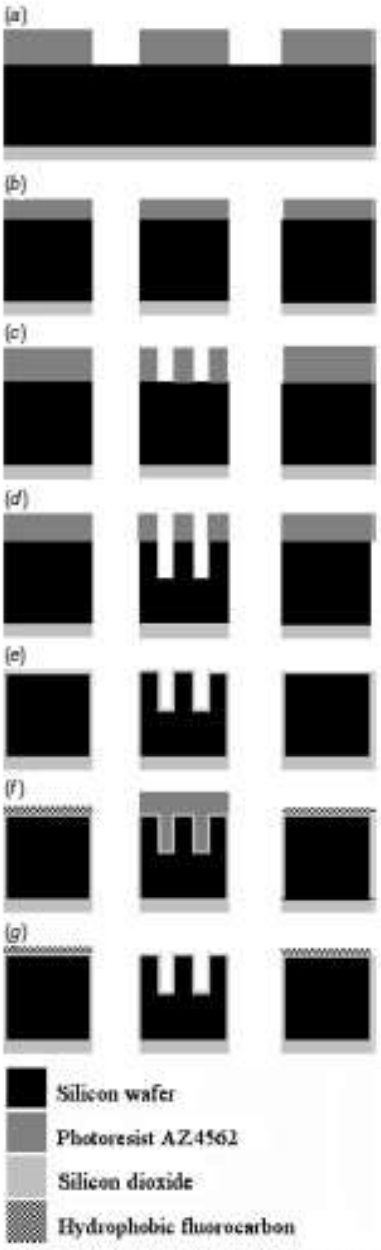

Figure 4. Microfabrication steps used for the fabrication of the anode and cathode silicon-based microchannels.

fuel cell power density as a function of input fuel flow variation at constant air flow (30 sccm) for two different fuel cell areas: $A = 0.39\ \text{cm}^2$ and $0.18\ \text{cm}^2$.

3. Microfabrication

High resistivity (4500 Ω cm) silicon substrates (Siltronix, France) having a 3 inch diameter and a thickness of 380 μm were used to prepare the microfluidic and gas microchannels for the anode and the cathode. The critical steps of the process

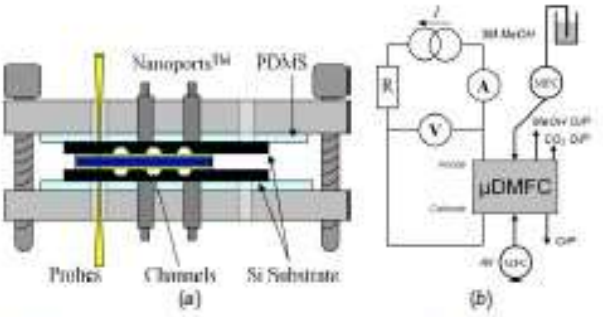

Figure 5. (*a*) Measurement set-up, and (*b*) microfluidic, gas and electrical circuits used for the experiments.

are illustrated in figure 4. A PECVD silicon dioxide film was deposited onto one wafer surface to protect it during plasma etching of the rear side of the wafer. A first photoresist (PR) layer (AZ4562) calibrated to have a thickness of 16 μm was spin-coated to make thru-holes in the Si wafer (see figure 4(*a*)). The Si wafer was etched using a successive etch/passivation DRIE comprising SF_6 etch cycles and C_4F_8 passivation cycles [38, 39] in a plasma etcher (Surface Technology Systems, UK) in order to have highly vertical sidewalls. Just prior to thru-hole formation (50 min corresponding to an etch rate of 7.2 μm min^{-1}), the wafer was removed and fixed onto an additional silicon support wafer in order to prevent the leakage of helium coolant gas upon thru-hole completion after etching the final 20 μm of silicon. Plasma etching was maintained until all thru-holes penetrated the wafer (see figure 4(*b*)). The first PR layer was then removed using successive washes of acetone, 2-propanol and de-ionized water followed by a H_2SO_4:H_2O_2 (vol:vol 50:50) solution cleaning step. A second PR (AZ4562) layer was then spin-coated in order to fabricate the fuel and gas microchannels (see figure 4(*c*)). These microchannels were also fabricated using the successive etch/passivation DRIE process (see figure 4(*d*)). The second PR layer was removed in the same manner as the first PR layer following plasma etching. The silicon surface was then covered by a native oxide layer following the H_2SO_4:H_2O_2 solution cleaning step (figure 4(*e*)). A third PR layer was then prepared in order to cover the anode channel areas. A ~1 μm thick hydrophobic fluorocarbon layer was then deposited onto the wafer surface using a C_4F_8-based plasma which is usually used for passivation mode in a successive etch/passivation DRIE process (figure 4(*f*)–(*g*)). The same process was used for the air-side wafer except that no masking was used to protect the cathode microchannels which we rendered hydrophobic.

4. Results and discussions

Figure 5 shows the microfluidic/electrical test set-up that was developed for the characterization of the fuel cells. The microfluidic/gas inputs/outputs were implemented using Nanoport™ connections (Upchurch Scientific, USA). Mass flow controllers were employed to control the fuel flow and the air flow. The silicon wafers, diffusion layers, electrodes and Nafion®117-based PEM were stacked as shown in figure 5(*a*)

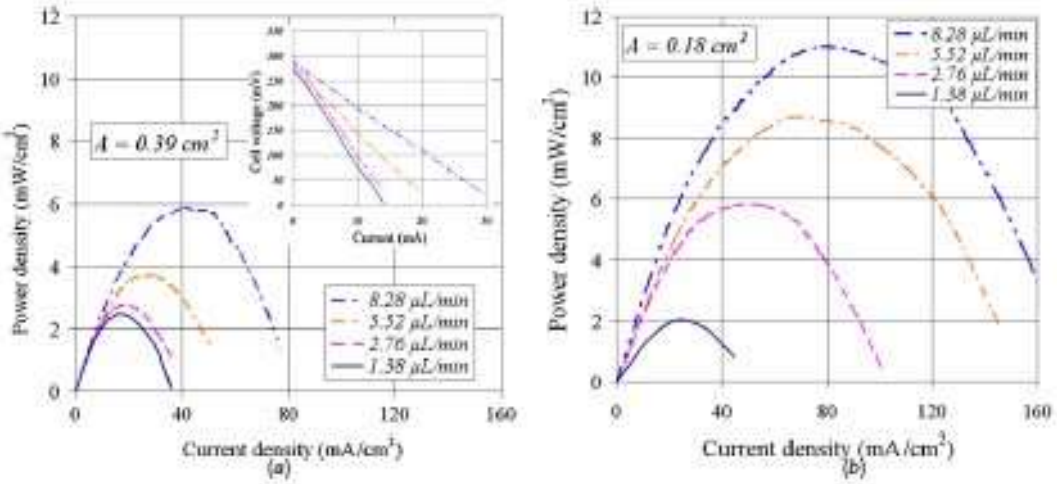

Figure 6. Fuel flow variation: (*a*) output power density versus current density at $A = 0.39$ cm^2; the inset shows current–voltage variation. (*b*) Output power density versus current density at $A = 0.18$ cm^2 (constant air flow rate of 30 sccm). Fuel cell parameters: (fuel-side) $w_{\mu a} = 50$ μm, $h_{\mu a} = 100$ μm, $d_{da} = 235$ μm (GDL-24 BC); (air-side) $w_{\mu c} = 200$ μm, $h_{\mu c} = 150$ μm, $d_{dc} = 400$ μm (LT-1400).

and held together by two rigid acrylic glass plates (thickness = 0.5 cm) containing thru-holes to enable alignment via the passage of the Nanoport™ connectors. Polydimethylsiloxane (PDMS) sheets (0.5 mm) were employed between the acrylic glass plates and silicon wafers to prevent the silicon wafers from cleaving. A 235 μm thick GDL-24 BC supplied by (SGL Carbon, Germany) was used as the anode diffusion layer. For the air diffusion layer, a commercial gas diffusion layer LT-1400 (E-TEK, USA) was employed; this had a thickness of 400 μm. Commercial gold mesh sheets (Goodfellow, UK) were employed as the collector electrodes for both anode and cathode; the wire diameter was 60 μm and the average space was 250 μm. Figure 5(*b*) shows the combined electrical, microfluidic and gas circuits. The electrical circuit employed a current source (0–50 mA), 3441 A digital multi-meters (Agilent, USA). The microfluidic and gas supply employed plastic tubing (OD = 1587 μm; ID = 762 μm) supplied from Cluzeau (France) which was connected to the Nanoport™ on the fuel- and air-sides of the silicon wafers. In terms of mass flow control, the force fed fuel flow rate was controlled by an IPC4 high-precision multi-channel dispenser peristaltic pump (Ismatec, Switzerland) having a flow rate range of 0–39 μL min^{-1} whilst an STEC SEC-7300 mass flow controller (Horiba, Japan) was employed for the air having a mass flow range of 2–50 sccm. Measurements were taken in the following sequence: (i) fuel flow variation at constant air flow for different cell areas, (ii) air flow variation at constant fuel flow for different cell areas and (iii) fuel flow variation at constant air flow for different microchannel cross-sections. All measurements were taken at room temperature. The output power density as a function of current density data was evaluated from the measured current (mA) versus voltage (mV) characteristics; measurements were repeated several times by (i) repeated *I–V* measurements and (ii) by dismantling and reassembling the microfluidic set-up to ensure repeatability of the electrical results. Statistical error bars are not included but we estimate the error in the output power density to be approximately $\pm$ 0.2 mW cm^{-2}.

Figure 6 shows the output power density of fuel cells having a surface area equal to 0.39 cm^2 and 0.18 cm^2 when varying the fuel flow rate from 1.38 μL min^{-1} to 8.28 μL min^{-1} whilst keeping the air flow rate at a constant 30 sccm; the air flow rate was initially held at 30 sccm to ensure no mass flow problems at the cathode. Figure 7 shows the output power density of fuel cells having a surface area equal to 0.39 cm^2 and 0.18 cm^2 when varying the air flow rate from 5 sccm to 30 sccm whilst keeping the fuel flow rate at a constant 2.76 μL min^{-1}. Figure 8 shows the effect on the output power density when reducing the microchannel height for a fuel cell having a surface area equal to 0.3 cm^2 when varying the fuel flow rate from 1.38 to 5.52 μL min^{-1} at a constant air flow rate of 10 sccm.

Our results should be analysed and compared to each other and to those obtained using silicon-based microtechnology in the literature [17–30]. To do this, we calculate a figure of merit termed the fuel use efficiency [40] from the current density (mW cm^{-2}) at maximum power density, the active cell surface (cm^2) and the fuel flow rate (mol s^{-1}). Table 2 shows a summary of results and a calculation of the fuel use efficiencies for the results presented here and those calculated from results published in the literature; note that values are only shown where numbers could be extracted. There are several important observations to be made from table 2. First, let us consider our results; if we compare output power densities and fuel use efficiencies, then a smaller cell (0.18 cm^2) results in a higher output power density over the fuel flow range (with the exception of 1.38 μL min^{-1}). However, a larger cell (0.39 cm^2) results in improved fuel use efficiency (15%) at a lower fuel flow rate (1.38 μL min^{-1}). In both fuel cell surfaces ($h_{\mu a} = 100$ μm), the fuel use efficiency decreases with increasing fuel flow rate. Using an anode microchannel height of 50 μm, our best power density result of 12.5 mW cm^{-2} at a fuel flow rate of 5.52 μL min^{-1} (3 M)

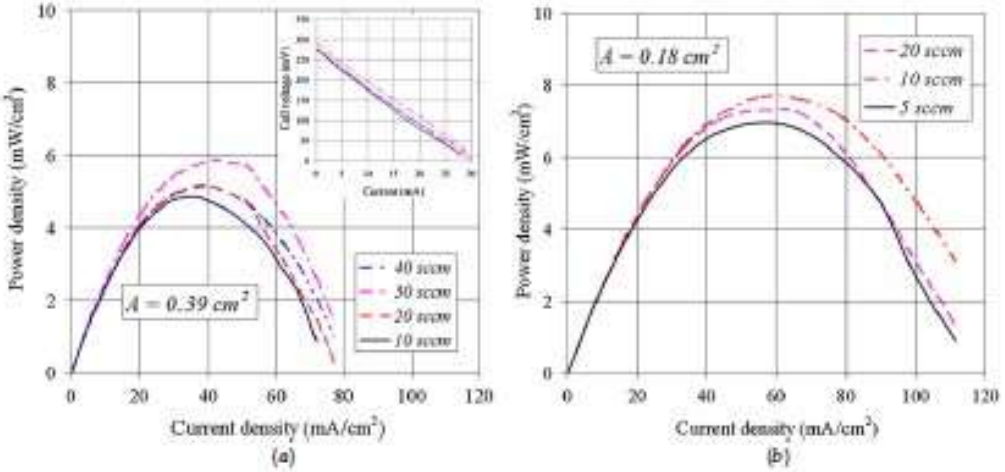

Figure 7. Air flow variation: (*a*) output power density versus current density at $A = 0.39$ cm^2; the inset shows current–voltage variation. (*b*) Output power density versus current density at $A = 0.18$ cm^2 (constant fuel flow rate of 2.77 μL min^{-1}). Fuel cell parameters: (fuel-side) $w_{\mu a} = 50$ μm, $h_{\mu a} = 100$ μm, $d_{\text{fa}} = 235$ μm (GDL-24 BC); (air-side) $w_{\mu c} = 200$ μm, $h_{\mu c} = 150$ μm, $d_{\text{fc}} = 400$ μm (LT-1400).

Table 2. Summary of results and comparison with those published in the literature.

$P_{\max}$ (mW cm^{-2})	A (cm^2)	Q_{fa} (μL min^{-1})	Fuel use efficiency (%) [40]	Reference
4.3	0.3	1.38	20.1	This work[a]
7.9	0.3	2.76	17.7	This work[a]
12.5	0.3	5.52	14.1	This work[a]
2	0.18	1.38	11.7	This work[b]
5.8	0.18	2.76	11.3	This work[b]
8.7	0.18	5.52	7.5	This work[b]
11	0.18	8.28	5.9	This work[b]
2.45	0.39	1.38	15	This work[b]
2.8	0.39	2.76	10	This work[b]
3.7	0.39	5.52	6.3	This work[b]
5.8	0.39	8.28	6.5	This work[b]
10.6	0.18	1.38	27	Model [33]
9.2	0.3	1.38	37.6	Model [33]
8	0.39	1.38	40	Model [33]
12	0.25	2000	0.2	[17]
14.3	1.6	283	4.7	[18]
0.29	0.25	0.166	6.5	[20]
16	1.625	283	2.2	[22]
0.38	2.64	1000	0.1	[23]
34	1	800	1.9	[26]
8.08	0.476	600	0.2	[28]
4.9	1	10	15.5	[29]

[a] $h = 50$ μm;
[b] $h = 100$ μm.

corresponds to 14.1% fuel use efficiency; our best result in terms of fuel use efficiency is 20.1% achieved at a fuel flow rate of 1.38 μL min^{-1} resulting in a maximum power density of 4.3 mW cm^{-2}. As discussed previously, it should be noted that reducing h by a factor of 2 increased the microchannel pressure by ~3.55 times, thus increasing the possibility of fuel leaks and associated reduced performances. We can now compare our results with the modelling (see figure 3). The modelling

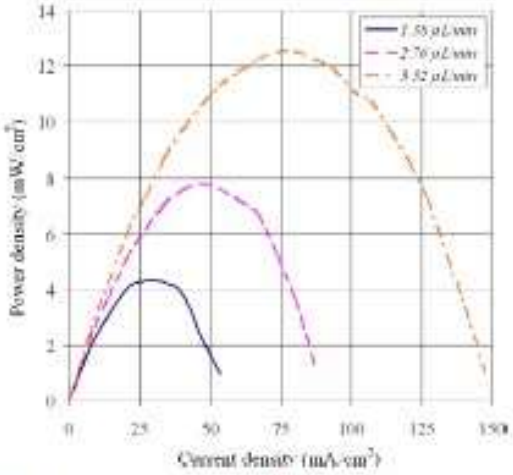

Figure 8. Anode microchannel height variation: output power density versus current density at $A = 0.3$ cm^2. Fuel cell parameters: (fuel-side) $w_{\mu a} = 50$ μm, $h_{\mu a} = 50$ μm, $d_{\text{fa}} = 235$ μm (GDL-24 BC); (air-side) $w_{\mu c} = 200$ μm, $h_{\mu c} = 150$ μm, $d_{\text{fc}} = 400$ μm (LT-1400).

predicts the correct trends observed here: a large cell resulting in a lower output power density (figures 3(*c*) and (*d*)). A calculation of the fuel use efficiency from the modelling also predicts the observations here. However, the modelling predicts higher power densities, higher current densities and fuel use efficiencies than those observed here, possibly due to the fact that carbon dioxide bubble formation and fuel leaks, for example, are not taken into account. The model also fails to predict the importance of the microchannel height h on the cell performance which we observe here; this is due to the fact that the pressure drop along the microchannel is not taken into account in the model [33]. Reducing the microchannel height leads to a higher velocity in the microchannel and an

increased pressure and thus a higher mass transfer; indeed our best performance obtained using $h = 50$ μm and $w = 100$ μm corresponds to the optimum aspect ratio reported by Wong *et al* [26] using larger microchannels and higher fuel flow rates.

Comparisons must also be made with performances in the literature although one should note that microDMFC characterization involves many parameters and direct comparison is not always evident. Despite this, we have extracted where possible the power density and the fuel use efficiency, based on [40]. We can compare our results to groups who use fuel flow rates >100 μL min^{-1} and groups <100 μL min^{-1}. In the former we have Kelley *et al* [17] who achieved a power density of 12 mW cm^{-2} at a rather large fuel flow rate of 2000 μL min^{-1}. Yeom *et al* [23] achieved 0.38 mW cm^{-2} at a fuel flow rate of 1000 μL min^{-1} and Yen *et al* [18] achieved 47.2 mW cm^{-2} for dry-etched silicon microchannels (750 μm width by 400 μm depth) operating at 60 °C, but this fell to 12 mW cm^{-2} at room temperature for a fuel flow rate of 283 μL min^{-1} corresponding to a fuel use efficiency of 4.7%. However, a notable recent result is Wong *et al* [26] who demonstrated a power output of 34 mW cm^{-2} for a 1 cm^2 serpentine silicon-microchannel-based system at a fuel flow rate of 800 μL min^{-1} (fuel use efficiency = 1.9%); this group also showed that a smaller microchannel height coupled with a serpentine microchannel rather than parallel channels improves cell performances, but the results were again generated at a relatively high fuel flow rate of 800 μL min^{-1}. Zhang *et al* [28], using silicon microchannels in a novel microblock array, achieved a room temperature power density of 8.08 mW cm^{-2} at a fuel flow rate of 600 μL min^{-1} (fuel use efficiency = 0.2%). In general, the use of a high fuel flow rate to achieve a high power output results in lower fuel use efficiency. In terms of low fuel flow rate and reduced cell area, Wozniack *et al* [20] used a very low flow rate of 0.16 μL min^{-1} to achieve 0.29 mW cm^{-2} achieving a fuel use efficiency of 6.5%, and Esquivel *et al* [27] used a flow rate of 2 μL min^{-1} (estimated from 100 μL over 50 min use) to obtain 10 mW cm^{-2}. In addition, Motokawa *et al* [21] demonstrated a cell having a surface of 0.018 cm^2 achieving 0.78 mW cm^{-2} at a low fuel flow rate of 10 μL min^{-1} and Liu *et al* [29] also used a fuel flow rate of 10 μL min^{-1} to obtain 4.9 mW cm^{-2}.

High performance micro fuel cells can be realized by enhancing the fuel use efficiency. If the required power output can be obtained efficiently with lower fuel supply, a simpler cell could be envisaged via the elimination of devices such as pumps; lower energy consumption could be achieved in the cell and an accordingly higher effective performance is realized. The flux φ_{da}, which is the flux of supplied fuel from the microchannels to the diffusion layer, is dependent on the amount of fuel which is consumed in reaction and crossover flux φ_m (equation (3)). The ratio of crossover fuel shown in equation (4) and consumed fuel in the reaction is near constant when a maximum output is produced from the MEA at a certain fuel concentration. The supplied fuel to the microchannels can be used more efficiently if a minimum amount of fuel is supplied to maintain the fuel concentration. With longer channels however, the fuel flux from microchannels to the diffusion layer gradually decreases along the microchannel, i.e. the cell surface; it is thus difficult to maintain a certain fuel concentration all over the cell surface. Using a larger microchannel geometry is counter to miniaturization of the cell which requires the cell to be smaller and the channels to be shorter. Constant fuel concentration can then be maintained using a small amount of fuel flow all over the cell surface.

5. Conclusions

Silicon microsystems have been successfully employed to characterize the room temperature performances of miniaturized micro direct methanol fuel cells having small surface areas (<0.4 cm^2) at low forced input fuel flow rates (<10 μL min^{-1}). A state-of-the-art fuel use efficiency of 20.1% was observed at a fuel flow rate of 1.38 μL min^{-1} for a fuel cell operating at room temperature; comparison with the literature reveals that this value is an improvement on the previous work. Fuel and oxidant were circulated using serpentine microchannels etched in silicon wafers; the microchannels had dimensions of the order of 50–100 μm. A rigid microfluidic/electrical test set-up was developed which combines silicon wafers, diffusion layers, electrodes and a commercial proton exchange membrane set-up which gave highly repeatable results. A state-of-the-art room temperature power output of 12.5 mW cm^{-2} was measured for a fuel cell having an active area equal to 0.3 cm^2 at a fuel flow rate of 5.52 μL min^{-1} at 300 K although in this case the fuel use efficiency fell to 14.1%. The study showed that improved cell performances in terms of power density can be achieved at low flow rates (<10 μL min^{-1}) by (i) reducing the fuel cell area and (ii) reducing the microchannel cross-section. The study also revealed that higher fuel use efficiencies can be obtained at a lower fuel flow rate. In terms of cell surface, agreement is found between the results and the trends predicted by an analytical model; however, the model ignores the pressure gradient along the anode microchannel and thus fails to predict the enhanced performances observed here when the microchannel height is reduced. Our results indicate that the output is more sensitive to fuel flow than air flow over the test range and that a maximum power density was obtained for a smaller surface and shallower microchannels.

Acknowledgments

The authors thank Dr Toru Chiba and Dr Akira Takahashi (Sharp Corporation) for their support of the project. We also thank Professor Alain Cappy (Head of IEMN) for allowing the work to be carried out at IEMN.

References

[1] Steele B C H and Heinzel A 2001 Materials for fuel-cell technologies *Nature* **414** 345–52
[2] Dyer C K 2002 Fuel cells for portable applications *J. Power Sources* **106** 31–4

[3] Arico A S, Srinivasan S and Antonucci V 2001 DMFCs: from fundamental aspects to technology development *Fuel Cells* **1** 133–61

[4] Kamarudin S K, Daud W R W, Ho S L and Hasran U A 2007 Overview on the challenges and developments of micro-direct methanol fuel cells (DMFC) *J. Power Sources* **163** 743–54

[5] Heinzel A and Barragán V M 1999 A review of the state-of-the-art of the methanol crossover in direct methanol fuel cells *J. Power Sources* **84** 70–4

[6] Gurau B and Smotkin E S 2002 Methanol crossover in direct methanol fuel cells: a link between power and energy density *J. Power Sources* **112** 339–52

[7] Lu G Q and Wang C Y 2004 Electrochemical and flow characterization of a direct methanol fuel cell *J. Power Sources* **134** 33–40

[8] Lundin M D and McCready M J 2007 Reduction of carbon dioxide gas formation at the anode of a direct methanol fuel cell using chemically enhanced solubility *J. Power Sources* **172** 553–9

[9] Litterst C, Eccarius S, Hebling C, Zengerle R and Koltay P 2006 Increasing μDMFC efficiency by passive CO_2 bubble removal and discontinuous operation *J. Micromech. Microeng.* **16** S248–53

[10] Scott K, Taama W M, Argyropoulos P and Sundmacher K 1999 The impact of mass transport and methanol crossover on the direct methanol fuel cell *J. Power Sources* **83** 204–16

[11] Schultz T and Sundmacher K 2006 Mass, charge and energy transport phenomena in a polymer electrolyte membrane (PEM) used in a direct methanol fuel cell (DMFC): modelling and experimental validation of fluxes *J. Membr. Sci.* **276** 272–85

[12] Jewett G, Guo Z and Faghri A 2007 Water and air management systems for a passive direct methanol fuel cell *J. Power Sources* **168** 434–46

[13] Squires T M and Quake S R 2005 Microfluidics: fluid physics at the nanoliter scale *Rev. Mod. Phys.* **77** 977–1026

[14] Choban E R, Markoski L J, Wieckowski A and Kenis P J A 2004 Microfluidic fuel cell based on laminar flow *J. Power Sources* **128** 54–60

[15] Bazylak A, Sinton D and Djilali N 2005 Improved fuel utilization in microfluidic fuel cells: a computational study *J. Power Sources* **143** 57–66

[16] Sun M H, Velve Casquillas G, Guo S S, Shi J, Ji H, Ouyang Q and Chen Y 2007 Characterization of microfluidic fuel cell based on multiple laminar flow *Microelectron. Eng.* **84** 1182–5

[17] Kelley S C, Deluga G A and Smyrl W H 2000 A miniature methanol/air polymer electrolyte fuel cell *Electrochem. Solid-State Lett.* **3** 407–9

[18] Yen T J, Fang N, Zhang X, Lu G Q and Wang C Y 2003 A micro methanol fuel cell operating at near room temperature *Appl. Phys. Lett.* **83** 4056–8

[19] Seo Y H and Cho Y H 2003 A miniature direct methanol fuel cell using platinum sputtered microcolumn electrodes with limited amount of fuel *16th Ann. Int. Conf. on Micro Electro Mechanical Systems, 2003. MEMS-03 (Kyoto) (IEEE)* pp 375–8

[20] Wozniak K, Johansson D, Bring M, Sanz-Velasco A and Enoksson P 2004 A micro direct methanol fuel cell demonstrator *J. Micromech. Microeng.* **14** S59–63

[21] Motokawa S, Mohamedi M, Momma T, Shoji S and Osaka T 2004 MEMS-based design and fabrication of a new concept micro direct methanol fuel cell *Electrochem. Commun.* **6** 562–5

[22] Lu G Q, Wang C Y, Yen T J and Zhang X 2004 Development and characterization of a silicon-based micro direct methanol fuel cell *Electrochim. Acta* **49** 821–8

[23] Yeom J, Mozsgai G Z, Flachsbart B R, Choban E R, Asthana A, Shannon M A and Kenis P J A 2005 Microfabrication and characterization of a silicon-based millimeter scale, PEM fuel cell operating with hydrogen, methanol, or formic acid *Sensors Actuators* B **107** 882–91

[24] Yao S-C, Tang X, Hsieh C-C, Alyousef Y, Vladimer M, Fedder G K and Amon C H 2006 Micro-electro-mechanical systems (MEMS)-based micro-scale direct methanol fuel cell development *Energy* **31** 636–49

[25] Jiang Y, Wang X, Zhong L and Liu L 2006 Design, fabrication and testing of a silicon-based air-breathing micro direct methanol fuel cell *J. Micromech. Microeng.* **16** S233–39

[26] Wong C W, Zhao T S, Ye Q and Liu J G 2005 Experimental investigations of the anode flow field of a micro direct methanol fuel cell *J. Power Sources* **155** 291–6

[27] Esquivel J P, Sabate N, Santander J, Torres N and Cane C 2008 Fabrication and characterization of a passive silicon-based direct methanol fuel cell *Microsyst. Technol.* **14** 535–41

[28] Zhang Y, Lu J, Shimano S, Zhou H and Maeda R 2007 Development of MEMS based direct methanol fuel cell with high power density using nanoimprint technology *Electrochem. Commun.* **9** 1365–8

[29] Liu X, Suo C, Zhang Y, Wang X, Sun C, Li L and Zhang L 2006 Novel modification of Nafion117 for a MEMS-based micro direct methanol fuel cell (μDMFC) *J. Micromech. Microeng.* **16** S226–32

[30] Zhang Q, Wang X, Zhong L, Zhou Y, Qiu X and Liu L 2008 A silicon based micro direct methanol fuel cell with microblocks in anode structure *Proc. MEMS (Tucson, AZ, USA, 2008)* pp 972–5

[31] Quéré D 1998 Drops at rest on a tilted plane *Langmuir* **14** 2213–6

[32] Schiffter H and Lee G 2006 Single-droplet evaporation kinetics and particle formation in an acoustic levitator *J. Pharm. Sci.* **96** 2274–83

[33] Guo H and Ma F 2004 2D analytical model of a direct methanol fuel cell *Electrochem. Commun.* **6** 306–12

[34] Argyropoulos P, Scott K, Shukla A K and Jackson C 2003 A semi-empirical model of the direct methanol fuel cell performance: Part I. Model development and verification *J. Power Sources* **123** 190–9

[35] García B L, Sethuraman V A, Weidner J W, White R E and Dougal R 2004 Mathematical model of a direct methanol fuel cell *J. Fuel Cell Sci. Technol.* **1** 43–8

[36] Chen R and Zhao T S 2005 Mathematical modeling of a passive-feed DMFC with heat transfer effect *J. Power Sources* **152** 122–30

[37] Scott K, Jackson C and Argyropoulos P 2006 A semi empirical model of the direct methanol fuel cell: Part II. Parametric analysis *J. Power Sources* **161** 885–92

[38] McAuley S A, Ashraf H, Atabo L, Chambers A, Hall S, Hopkins J and Nicholls G 2001 Silicon micromachining using a high density plasma source *J. Phys. D: Appl. Phys.* **34** 2769–74

[39] Lärmer F and Schilp A 1992 Method for anisotropically etching silicon *German Patent Specification* DE4241045

[40] O'Hayre R, Cha S-W, Colelle W and Prinz F B 2006 *Fuel Cell Fundamentals* (New York: Wiley)